Design and evaluation of a novel sub-scaffold dental implant system based on the osteoinduction of micro-nano bioactive glass

Fujian Zhao[1], Zhen Yang[2,3], Lu Liu[2,3], Dafu Chen[4], Longquan Shao[1,], Xiaofeng Chen[2,3,*]*

Key Words:
alveolar ridge augmentation; micro-nano bioactive glass; osteoinduction; sub-scaffold dental implant system

From the Contents

ABSTRACT

Alveolar ridge atrophy brings great challenges for endosteal implantation due to the lack of adequate vertical bone mass to hold the implants. To overcome this limitation, we developed a novel dental implant design: sub-scaffold dental implant system (SDIS), which is composed of a metal implant and a micro-nano bioactive glass scaffold. This implant system can be directly implanted under mucous membranes without adding any biomolecules or destroying the alveolar ridge. To evaluate the performance of the novel implant system in vivo, SDISs were implanted into the sub-epicranial aponeurosis space of Sprague–Dawley rats. After 6 weeks, the SDIS and surrounding tissues were collected and analysed by micro-CT, scanning electron microscopy and histology. Our results showed that SDISs implanted into the sub-epicranial aponeurosis had integrated with the skull without any mobility and could stably support a denture. Moreover, this design achieved alveolar ridge augmentation, as active osteogenesis could be observed outside the cortical bone. Considering that the microenvironment of the sub-epicranial aponeurosis space is similar to that of the alveolar ridge, SDISs have great potential for clinical applications in the treatment of atrophic alveolar ridges. The study was approved by the Animal Care Committee of Guangdong Pharmaceutical University (approval No. 2017370).

***Corresponding authors:**
Xiaofeng Chen,
chenxf@scut.edu.cn;
Longquan Shao,
shaolongquan@smu.edu.cn.

http://doi.org/10.3877/cma.j.issn.2096-112X.2020.01.008

How to cite this article:
Zhao, F.; Yang, Z.; Liu, L.; Chen, D.; Shao, L.; Chen, X. Design and evaluation of a novel sub-scaffold dental implant system based on the osteoinduction of micro-nano bioactive glass. *Biomater Transl.* **2020**, *1*(1), 82-88.

Introduction

When natural teeth are missing, a prosthesis is used to restore masticatory function. Options include a fixed denture, removable denture, or dental implant. Considering the disadvantages of fixed and removable dentures, such as normal tooth damage and strong foreign body sensation, dental implants are the current standard for the replacement of missing teeth. Implants have been widely applied in a variety of cases including surgical replacement of lost teeth or restoration of oral function.[1] Although different types of implants have been developed previously, endosteal implants are currently the most widely used.[2]

However, endosteal implants still have some shortcomings. For example, in the event of inflammation developing around the implant, a dental implant may lose stability due to the small contact area between the implant and the bone, which is the main reason for dental implant failure.[3] Some surgical complications such as destruction of the tooth groove nerve or maxillary sinus will also occur because the dental implant is implanted in the jaw. Moreover, a significant factor that limits the clinical application of an endosteal implant is the restrictive necessity for alveolar bone mechanical support.[4] Successful implant placement requires sufficient alveolar bone volume in order to ensure implant stability and osseointegration, but the extraction of teeth will result in loss of alveolar ridge width and height within three years.[5] This bone loss is exacerbated if the tooth is removed traumatically or if there are pre-existing endodontic or periodontal pathologies. Eventually, the height of the alveolar ridge will be insufficient to contain the length of the implant.

To overcome these problems, this study puts forward a novel dental implant design: the sub-scaffold dental implant system (SDIS), which is implanted just below

the mucous membranes, without destroying the jaw. This implant system is composed of a metal implant and an osteogenic scaffold. The metal implant is used to attach the dentures, while the osteogenic scaffold will eventually transform into bone on the alveolar ridge, augmenting vertical bone at the same time. Vertical ridge augmentation remains a challenge in reconstruction of the atrophic maxilla and mandible. Various biomaterials and techniques have been developed to solve this problem including onlay bone grafts, guided bone regeneration, bone splitting for ridge expansion, distraction osteogenesis, revascularised flaps and sinus floor elevation via a lateral approach.[6] Every surgical procedure has its advantages and disadvantages and it is difficult to demonstrate that one surgical procedure offers better outcomes than another.[7, 8] Autografts are considered to be the 'gold standard' grafting material for reconstruction of the vertical ridge.[9] However, they have certain drawbacks, including the necessity for a second stage surgery, the high morbidity and blood loss at the donor site, high resorption rate of the graft and limited bone availability.[10]

The use of bone formation materials instead of autografts is a better choice to achieve vertical ridge augmentation.[11, 12] Recently, some studies have reported augmentation of the alveolar ridge by using osteogenic materials including tricalcium phosphate,[13-15] hydroxyapatite,[16] hydrogel[17, 18] and anorganic bovine bone.[19, 20] However, most of these methods required the addition of biomolecules or rapid establishment of a blood supply from the jaw by creating bone defects, which would not be suitable for actual clinical application or would result in additional trauma.

In our dental implant design, new bone is expected to be formed outside of the alveolar ridge without creating any bone defect. This requires the biomaterial to have excellent bone-forming ability. Micro-nano bioactive glass (MNBG) is a good choice for this application due to its enhanced biocompatibility, osteoconductive and osteoinductive properties.[21] It has been widely applied in the clinic as a bone filler, bone repair material and adjuvant in bone grafts.[22] The gene activation function is one of its great features which distinguishes it from other bone repair materials. When it is in contact with body fluids, ions (Si, Ca, P, etc.) can be quickly released from bioactive glass, which activate osteogenesis-related signalling pathways.[23] In our current work, the SDIS was developed by fabricating an MNBG scaffold and metal implant. The SDISs were implanted into the sub-epicranial aponeuroses of Sprague-Dawley rats. After testing the denture repair effect, the presence of new bone formation was further investigated by micro-CT, scanning electron microscopy (SEM) and histology.

Methods

Fabrication of SDIS

Preparation of metal implants by selective laser melting

The SDIS was made up of two parts: a metal implant and an osteogenic scaffold. The metal implant was fabricated through a selective laser melting process. To fabricate the metal implants, 316 L stainless steel powders provided by Renishaw PLC (Wotton-under-Edge, UK), with a mean diameter of 30 μm, were used as raw material and the metal implant models were designed by computer-aided design (CAD). Selective laser melting was performed using EVOProject (Renishaw PLC) with an SPI red POWER 200 W ytterbium fibre laser, an automatic powder layering system, an argon gas protection system and a process control system. The surface topography of the stainless steel implant was tested by SEM (DSM 982-Gemini, Zeiss, Oberkochen, Germany).

Fabrication of MNBG scaffolds

MNBG microspheres, with a molar ratio of SiO_2:CaO:P_2O_5 = 80:15:5, were synthesised by the sol-gel co-template method according to our previous reports.[24] The initial paste for three-dimensional (3D) printing was prepared by mixing bioactive glass microspheres together with 10% polyvinyl alcohol (PVA) solution in a mass ratio of 1:1. The scaffolds were fabricated using a 4th generation 3D-Bioplotter system (EnvisionTEC GmbH, Gladbeck, Germany) under the guidance of supporting computer workstations. The desired scaffold models (10 mm × 10 mm × 1.8 mm) were designed by CAD. The paste was extruded through a conical plastic nozzle with an interior diameter of 200 μm with an interval between strands of 400 μm at room temperature. After drying at 30°C for two days, the scaffolds were cut into 8 mm diameter discs. Finally, a 1.8 mm diameter hole was made in the centre of each disc using a dental drill, which was used to accommodate the metal implant. The morphology of the scaffolds was observed using SEM.

Animal model

Six Sprague-Dawley rats (male, 200–250 g) were purchased from the Laboratory Animal Centre, South China Medical College and used as animal models to test the effect of implanting SDISs. All animal procedures were performed following a protocol approved by the Animal Care Committee of Guangdong Pharmaceutical University (approval No. 2017370) and adequate measures were taken to minimise pain and discomfort to the animals.

Surgical procedure

SDISs were implanted under the epicranial aponeurosis of the skull. Before animal surgery, the SDISs were assembled together and sterilised by gamma irradiation. After general anaesthesia with 10% chloral hydrate, the hair was shaved from the head of each rat. Then the cutaneous surface was disinfected with povidone iodine solution prior to the operation. A 1 cm long full depth incision was made on the calvaria in a coronal direction and the epicranial aponeurosis was separated from the bone surface by tunnelling dissection. One SDIS was inserted into the subgaleal space, which was then closed with sutures.

Evaluation of the repair effect

At 6 weeks after surgery, a 0.5 cm long full-depth incision was

1 Stomatological Hospital, Southern Medical University, Guangzhou, Guangdong Province, China; 2 Department of Biomedical Engineering, School of Materials Science and Engineering, South China University of Technology, Guangzhou, Guangdong Province, China; 3 National Engineering Research Center for Tissue Restoration and Reconstruction, South China University of Technology, Guangzhou, Guangdong Province, China; 4 Laboratory of Bone Tissue Engineering, Beijing Laboratory of Biomedical Materials, Beijing Research Institute of Orthopaedics and Traumatology, Beijing Jishuitan Hospital, Beijing, China.

made at the most prominent part of the skull, and the metal implant was exposed by blunt dissection. A stainless steel connecting rod (diameter 0.8 mm, length 4 mm) was used to connect the implant and a false tooth. One end of the connecting rod was inserted into a hole in the metal implant. Then, a plastic tooth was fixed onto the other end of the connecting rod.

A further 6 weeks after this procedure, all the animals were sacrificed using an overdose of sodium pentobarbital. The SDIS and surrounding bone tissue of the skull were harvested. All the tissues were fixed in 10% phosphate-buffered formalin for 5 days before analysis.

Micro-CT analysis

Specimens were examined by a micro-CT (ZKKS-MCT-SharpII, Zhongkekaisheng Medical Technology Co., Ltd., Guangzhou, China) operated at a voltage of 60 kVp and an electric current of 67 mA. The voxel size after reconstruction was 25 μm × 25 μm × 25 μm. Based on the micro-CT results, three-dimensional images were reconstructed by MIMICS® (interactive medical image control system; Materialise Co., Leuven, Belgium). Different substances were distinguished according to their different densities which were indicated by different colours.

Histological examination

Following micro-CT scanning, the samples were cut into two halves on the periphery of the metal implant. The metal-free part of each sample was decalcified in 10% ethylenediaminetetraacetic acid for 4 weeks and then embedded in paraffin parallel to the cut surface. Serial cross-sections of decalcified samples were sectioned for Masson's trichrome staining according to the manufacturer's instructions. Images were acquired using a Zeiss Axion light microscope (Axioskop 40 FL, Zeiss) and a colour video camera (Soft Imaging System, Muenster, Germany). All images were captured at 5× magnification using ImagePro software (Media Cybernetics, Rockville, MD, USA) and merged to give a composite of the whole slice.

Statistical analysis

Results are expressed as mean ± standard deviation (SD). Statistical analysis was carried out using one-way analysis of variance. A P value less than 0.05 was considered to be statistically significant.

Results

Characterization of SDIS

The SDIS consisted of two parts: a metal implant and an MNBG scaffold. The metal implant was composed of two parts with different functions, as shown in the CAD model (**Figure 1A**). The denture connection part was used to connect to the upper denture through the centre hole, which was similar to the neck of an endosteal implant. The fixation part was placed in contact with the newly-formed bone when SDIS was implanted and acted to fix the implant in place due to the large extension area. **Figure 1B** shows a digital image of two different surfaces of the metal implant. By comparing with the CAD model, it can be seen that the metal implant maintained the designed shape after the selective laser melting process. From the SEM image (**Figure 1C**), some print traces could be found on the surface of the metal implant. **Figure 1D** shows a digital image of the complete assembled SDIS. The MNBG scaffold was manufactured by the 3D printing method, then a hole with a diameter of 1.8 mm was created in the centre of the disc, which would match the denture connection part of the metal implant. An SEM image of the bioactive glass scaffold is shown in **Figure 1E** and the enlarged part of this image confirmed that the scaffold was composed of MNBG microspheres.

Clinical observations and denture repair effect

The SDIS was implanted into the sub-epicranial aponeurosis of

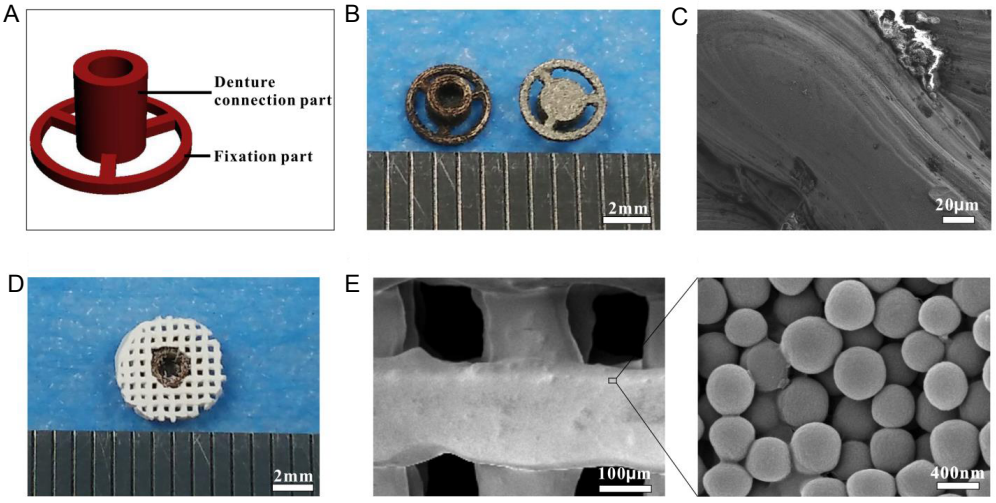

Figure 1. Composition and characterization of the SDIS. (A) A CAD model of the metal implant which consists of two parts: a denture connection part and a fixation part. (B) Digital photos of the two opposite surfaces of the metal implant, created by the SLM process. (C) SEM image of the metal implant. (D) Digital photo of the SDIS created by assembling the metal implant and MNBG scaffold together. (E) SEM image of the MNBG scaffold. Scale bars: 2 mm in B and D, 20 μm in C, 200 μm in E, 400 nm in enlarge part. CAD: computer-aided design; MNBG: micro-nano bioactive glass; SDIS: scaffold dental implant system; SEM: scanning electron microscopy; SLM: selective laser melting.

Sprague-Dawley rats as shown in **Figure 2A**. All animals used in this experiment survived for 6 weeks after implantation. SDISs were closely attached to the skull without any movement for one week. The ultimate purpose of this study was to develop a method to repair missing teeth using this dental implant design. The reparative effect of the SDIS was tested as shown in **Figure 2B**. The denture had firmly bonded to the connecting rod without any movement. The repair principle was shown in **Figure 2C**, which was similar to the endosteal implant. One end of the connecting rod was fixed into the centre hole of the metal implant, and the other end was fixed into the dental crown model.

New bone formation

Photographs of the SDIS and surrounding tissue are shown in **Figure 3A** and **B**. The residual materials had been combined closely with the skull without any mobility, and some blood vessels could be found on the surface of the residual bioactive glass scaffold. **Figure 3C** shows a 3D-reconstructed image, using micro-CT analysis, of the SDIS together with surrounding tissues and residual MNBG scaffold after implantation for 6 weeks. Some short rod-shaped scaffold fibres can be recognised on the surface of the residual material. The implant material had been closely integrated with the skull, as shown in the enlarged image.

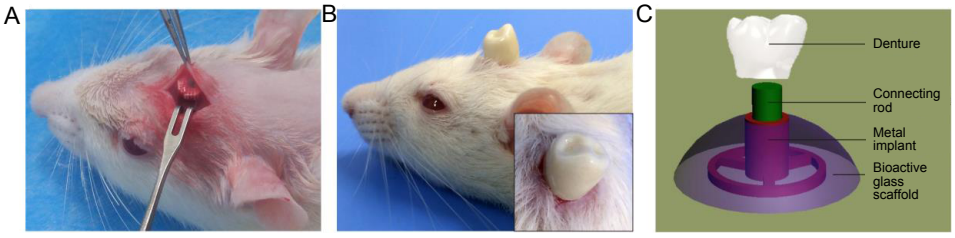

Figure 2. (A) Surgical placement of the SDIS implanted into the sub-epicranial aponeurosis; (B) Digital image of the repair effect and (insert) close-up of the top view; (C) Schematic illustration of the SDIS: the centre hole of the metal implant and the denture are joined together by a connecting rod. SDIS: scaffold dental implant system.

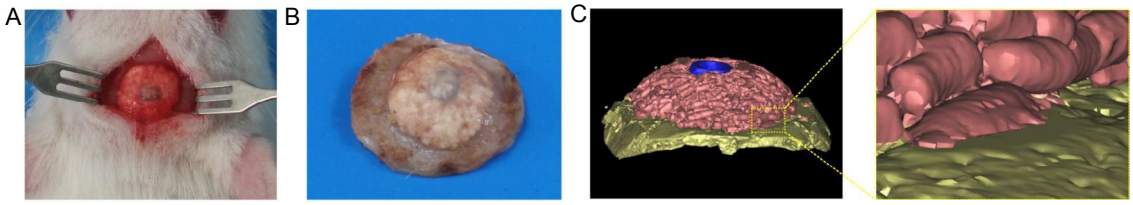

Figure 3. (A) Digital photo of the reparative effect. (B) Residual SDIS and surrounding bone tissue at week 6. (C) Micro-CT analysis of 3-dimensional reconstructed images of SDIS and surrounding tissue after implantation for 6 weeks. A magnified image of the join between implant and bone, showed good integration. Pink indicates residual bioactive glass scaffold, blue indicates the metal implant, and yellow indicates the skull. SDIS: scaffold dental implant system.

Since cortical bone has no blood vessels connecting with the bioactive glass scaffolds, the direction of colonisation of the soft tissue was from the periphery of the scaffolds to the interior. Therefore, different osteogenic stages could be observed at the interface between the bioactive glass scaffold and the cortical bone. The outcome of histological analysis after staining with Masson's trichrome is shown in **Figure 4**. In the central area, the scaffold gaps were filled with collagen-rich connective tissues alone, as the cells migrated at the last stage (**Figure 4A**). A white blank line could be observed between connective tissues and pericranium. Moreover, in some places, connective tissues had connected with the pericranium. In the area between the edge and the centre (**Figure 4B**), the MNBG scaffold was completely surrounded by collagen fibres, and in some cases the pericraniums had begun to be absorbed. In the edge area (**Figure 4C**), typical morphology of pre-lamellar bone was observed in close contact with the cortical bone surface. Osteocytes (red arrow) were present in the pre-lamellar bone. A small amount of connective tissue and residual MNBG scaffolds had been completely surrounded by newly-formed bone.

Discussion

After the loss of natural teeth, the alveolar bone heals and is covered by cortical bone. Due to the lack of mechanical stimulation, the alveolar ridge is gradually resorbed and becomes flat. In this experiment, the animal model provides a similar microenvironment to the alveolar ridge when natural tooth loss occurs. Moreover, the epicranial aponeurosis also exhibits similar tenacity to that of the alveolar ridge mucosa, so that MNBG scaffolds are subjected to a large pressing force. Consequently the animal model is consistent with the actual alveolar ridge atrophy which has been described in some reports.[25]

In order to repair missing teeth, different types of implants have been used in the clinic since the advent of dental implants. These include endosteal implants, subperiosteal implants, endodontic implants and stable transosteal implants.[26, 27] Although each type of implant has been popular for a period of time, endosteal implants (i.e., nail type implants) have become widely accepted in recent years. An endosteal implant is fixed into the alveolar ridge by making a hole which matches it. In this work, we designed a novel dental implant: the SDIS. Compared with traditional nail endosteal implants, the SDIS has the following advantages: (i) the

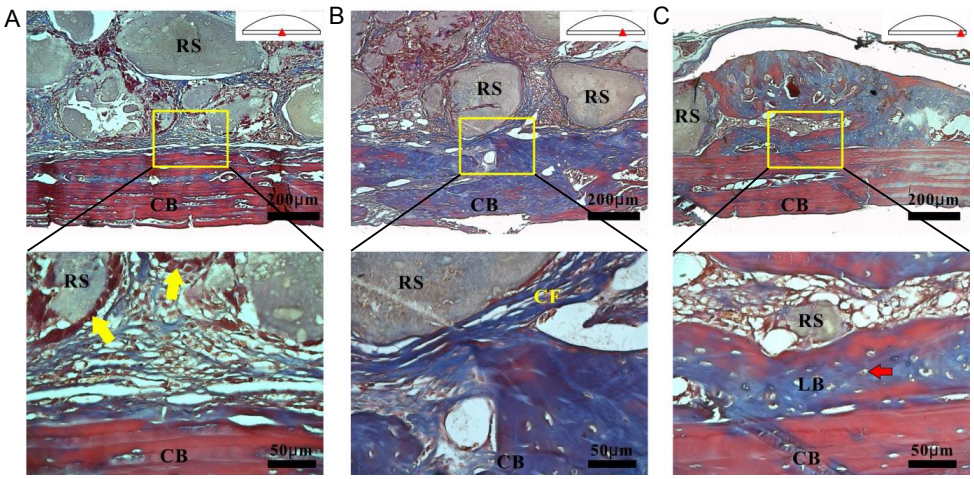

Figure 4. Histological analysis of the MNBG scaffolds and cortical bone after Masson's trichrome staining. (A, C) Centre and edge areas. (B) Area between edge and centre, as shown in the schematic diagram. The yellow boxes show the areas which are enlarged below. The yellow arrows indicate osteoblasts and the red arrow indicates an osteocyte. Scale bars: 200 μm (upper panel), 50 μm (lower panel). CB: cortical bone; CF: collagen fibres; LB: pre-lamellar bone; MNBG: micro-nano bioactive glass; RS: residual scaffolds.

surgical procedure is performed below the mucosa and does not destroy alveolar bone; (ii) due to the large contact area with the bone, the fixation part of the metal implant can act to disperse stress; (iii) this design can simultaneously replace multiple missing teeth by connecting the fixation parts together. In practical clinical application, the SDIS can be personalized manufacturing. Firstly, the morphology of the alveolar is needed to be reconstructed by using CT. Then the metal implants and BG scaffolds are fabricated by making full use of the advantages of 3D printing personalized manufacturing. Finally, the SDIS is installed on the surface of the alveolar after incising the mucoperiosteum of the alveolar.

Moreover, the most important advantage of the SDIS is that it can augment the alveolar ridge when the MNBG scaffold transforms into new bone. Currently, vertical bone augmentation for dental implant placement is one of the most challenging problems in implantology. Although several biomaterials have been used for alveolar ridge augment, such as tricalcium phosphate,[28] hydroxyapatite[16] and hydrogels,[17] the repair effect is still not satisfactory. Most of these studies require the creation of a bone defect (as the material has only bone conductive properties)[29] or the addition of biomolecules.[18, 30] In this study, vertical bone augmentation was achieved by using bioactive glass alone without adding any biomolecules.

The bone augmentation observed can be attributed to the osteoinductive property of bioactive glass.[31] Osteoinduction usually refers to the ability to form ectopic bone which means the material can be converted into new bone in non-bone sites (such as muscle and subcutaneous sites).[32] Whether bioactive glass has an osteoinductive property is a topic which has caused long-term controversy. Yuan et al.[33] reported that bone formation was found in pores of Bioglass® implanted in thigh muscles of dogs after 3 months. Miri et al.[34] injected dense collagen-Bioglass® hybrid gel scaffolds subcutaneously into adult rats, but only mineralised regions could be found and no bone formation was observed. Some other studies reported that they achieved ectopic bone formation with bioactive glass by adding BMP-2[35] or osteogenic cells.[36]

Urist et al.[37] thought that bone induction factors, osteogenic stem cells and a suitable osteogenic environment were the three conditions necessary for osteoinduction. In fact, osteoinduction in rodent subcutaneous models is a rare occurrence due to the lack of osteogenic stem cells at this site.[38] Previous studies also demonstrated that bioactive glass had no ectopic osteogenic potential in subcutaneous tissue,[39] but new bone could be found when bioactive glass was implanted subcutaneously together with osteogenic cells.[36] In our research, bioactive glass was kept in close contact with the pericranium which contains osteogenic stem cells.[40] The dissolution products of bioactive glass (Si, Ca and P) induced osteogenic differentiation of bone-marrow-derived adult stem cells (mesenchymal stem cells) into osteoblast-like cells, and the resulting cells produced mineralised matrix. This osteogenesis mechanism has been proven by *in vitro* experiments, which demonstrated that bioactive glass stimulates osteoprogenitor cells at the genetic level.[22]

In this experiment, the SDIS was placed directly onto the surface of the skull without any retention measures. However, the implants had unable to move after implanted for one week. This process could be divided into two stages: soft tissue combination and bone combination. In the early stage of implantation, the bioactive glass began to dissolve and combined with the soft tissue, which contributed to the formation of a hydroxycarbonate apatite layer on the surface of the bioactive glass.[41] With the formation of new bone, the pericranium was gradually resorbed and the newly-formed bone was directly connected to the cortical bone. This was confirmed by histological analysis which showed that new bone could be found at the edge of the scaffolds after 6 weeks. A similar study was also reported by Hench et al.[41] who demonstrated that bioactive glass could form a strong bond with bone.

In this study, a novel dental implant, the SDIS, was successfully

developed which was composed of a metal implant and an MNBG scaffold. The metal implant was used to connect dentures while the MNBG scaffold was used to form new bone on the alveolar ridge and augment the vertical bone at the same time. We implanted SDISs in the sub-epicranial aponeurosis of Sprague-Dawley rats. After 6 weeks the SDIS was combined closely with the skull without any mobility and the denture could bear certain lateral forces. In addition, active osteogenesis could be observed without the addition of any biomolecules or destruction of the alveolar ridge. The osteogenic stem cells in the pericranium may play a key role in mediating the osteoinductivity of MNBG scaffolds.

Author contributions

Conceptualization, methodology and original draft: FZ; study design: LS; data curation, investigation and validation: FZ, ZY and LL; Project administration: XC; funding acquisition: DC, XC and LS; manuscript review & editing: FZ and XC. All authors approved the final version of this manuscript.

Financial support

This study was financially supported by the National Key Research and Development Program of China (No. 2018YFC1106300), the China Postdoctoral Science Foundation (No. 2020M672732), the Natural Science Foundation of Guangdong Province of China (No. 2019A1515110480), the Medical Scientific Research Foundation of Guangdong Province of China (No. A2020107) and the Beijing Municipal Health Commission of China (Nos. BMHC-2019-9, BMHC-2018-4, PXM2020_026275_000002).

Acknowledgement

None.

Conflicts of interest statement

The authors declare no competing financial interest.

1. von Stein-Lausnitz, M.; Nickenig, H. J.; Wolfart, S.; Neumann, K.; von Stein-Lausnitz, A.; Spies, B. C.; Beuer, F. Survival rates and complication behaviour of tooth implant-supported, fixed dental prostheses: A systematic review and meta-analysis. *J Dent.* **2019**, *88*, 103167.
2. Bohner, L.; Hanisch, M.; Kleinheinz, J.; Jung, S. Dental implants in growing patients: a systematic review. *Br J Oral Maxillofac Surg.* **2019**, *57*, 397-406.
3. Liaw, K.; Delfini, R. H.; Abrahams, J. J. Dental implant complications. *Semin Ultrasound CT MR.* **2015**, *36*, 427-433.
4. Hansson, S.; Halldin, A. Alveolar ridge resorption after tooth extraction: A consequence of a fundamental principle of bone physiology. *J Dent Biomech.* **2012**, *3*, 1758736012456543.
5. Li, J.; Jansen, J. A.; Walboomers, X. F.; van den Beucken, J. J. Mechanical aspects of dental implants and osseointegration: A narrative review. *J Mech Behav Biomed Mater.* **2020**, *103*, 103574.
6. Chavda, S.; Levin, L. Human studies of vertical and horizontal alveolar ridge augmentation comparing different types of bone graft materials: a systematic review. *J Oral Implantol.* **2018**, *44*, 74-84.
7. Chiapasco, M.; Casentini, P.; Zaniboni, M. Bone augmentation procedures in implant dentistry. *Int J Oral Maxillofac Implants.* **2009**, *24* Suppl, 237-259.
8. McAllister, B. S.; Haghighat, K. Bone augmentation techniques. *J Periodontol.* **2007**, *78*, 377-396.
9. Ribeiro, M.; Fraguas, E. H.; Brito, K. I. C.; Kim, Y. J.; Pallos, D.; Sendyk, W. R. Bone autografts & allografts placed simultaneously with dental implants in rabbits. *J Craniomaxillofac Surg.* **2018**, *46*, 142-147.
10. Maiorana, C.; Poli, P. P.; Mascellaro, A.; Ferrario, S.; Beretta, M. Dental implants placed in resorbed alveolar ridges reconstructed with iliac crest autogenous onlay grafts: a 26-year median follow-up retrospective study. *J Craniomaxillofac Surg.* **2019**, *47*, 805-814.
11. Asa'ad, F.; Pagni, G.; Pilipchuk, S. P.; Giannì, A. B.; Giannobile, W. V.; Rasperini, G. 3D-printed scaffolds and biomaterials: review of alveolar bone augmentation and periodontal regeneration applications. *Int J Dent.* **2016**, *2016*, 1239842.
12. Sheikh, Z.; Sima, C.; Glogauer, M. Bone replacement materials and techniques used for achieving vertical alveolar bone augmentation. *Materials.* **2015**, *8*, 2953-2993.
13. Zigdon-Giladi, H.; Lewinson, D.; Bick, T.; Machtei, E. E. Mesenchymal stem cells combined with barrier domes enhance vertical bone formation. *J Clin Periodontol.* **2013**, *40*, 196-202.
14. Tamimi, F.; Torres, J.; Al-Abedalla, K.; Lopez-Cabarcos, E.; Alkhraisat, M. H.; Bassett, D. C.; Gbureck, U.; Barralet, J. E. Osseointegration of dental implants in 3D-printed synthetic onlay grafts customized according to bone metabolic activity in recipient site. *Biomaterials.* **2014**, *35*, 5436-5445.
15. Yang, J.; Kang, Y.; Browne, C.; Jiang, T.; Yang, Y. Graded porous β-tricalcium phosphate scaffolds enhance bone regeneration in mandible augmentation. *J Craniofac Surg.* **2015**, *26*, e148-153.
16. Singh, A.; Daing, A.; Anand, V.; Dixit, J. Two dimensional alveolar ridge augmentation using particulate hydroxyapatite and collagen membrane: A case report. *J Oral Biol Craniofac Res.* **2014**, *4*, 151-154.
17. Kinard, L. A.; Dahlin, R. L.; Lam, J.; Lu, S.; Lee, E. J.; Kasper, F. K.; Mikos, A. G. Synthetic biodegradable hydrogel delivery of demineralized bone matrix for bone augmentation in a rat model. *Acta Biomater.* **2014**, *10*, 4574-4582.
18. Kinard, L. A.; Dahlin, R. L.; Henslee, A. M.; Spicer, P. P.; Chu, C. Y.; Tabata, Y.; van den Beucken, J. J.; Jansen, J. A.; Young, S.; Wong, M. E.; Kasper, F. K.; Mikos, A. G. Tissue response to composite hydrogels for vertical bone augmentation in the rat. *J Biomed Mater Res A.* **2014**, *102*, 2079-2088.
19. Sheikh, Z.; Hamdan, N.; Ikeda, Y.; Grynpas, M.; Ganss, B.; Glogauer, M. Natural graft tissues and synthetic biomaterials for periodontal and alveolar bone reconstructive applications: a review. *Biomater Res.* **2017**, *21*, 9.
20. Titsinides, S.; Agrogiannis, G.; Karatzas, T. Bone grafting materials in dentoalveolar reconstruction: A comprehensive review. *Jpn Dent Sci Rev.* **2019**, *55*, 26-32.
21. Hu, Q.; Jiang, W.; Li, Y.; Chen, X.; Liu, J.; Chen, T.; Miao, G. The effects of morphology on physicochemical properties, bioactivity and biocompatibility of micro-/nano-bioactive glasses. *Adv Powder Technol.* **2018**, *29*, 1812-1819.
22. Jones, J. R. Review of bioactive glass: from Hench to hybrids. *Acta Biomater.* **2013**, *9*, 4457-4486.
23. El-Rashidy, A. A.; Roether, J. A.; Harhaus, L.; Kneser, U.; Boccaccini, A. R. Regenerating bone with bioactive glass scaffolds: A review of in vivo studies in bone defect models. *Acta Biomater.* **2017**, *62*, 1-28.
24. Zhao, F.; Xie, W.; Zhang, W.; Fu, X.; Gao, W.; Lei, B.; Chen, X. 3D printing nanoscale bioactive glass scaffolds enhance osteoblast migration and extramembranous osteogenesis through stimulating immunomodulation. *Adv Healthc Mater.* **2018**, *7*, e1800361.

25. Sheikh, Z.; Drager, J.; Zhang, Y. L.; Abdallah, M. N.; Tamimi, F.; Barralet, J. Controlling bone graft substitute microstructure to improve bone augmentation. *Adv Healthc Mater.* **2016**, *5*, 1646-1655.
26. Armitage, J.; Natiella, J.; Greene, G. Jr.; Meenaghan, M. An evaluation of early bone changes after the insertion of mental endosseous implants into the jaws of rhesus monkeys. *Oral Surg Oral Med Oral Pathol.* **1971**, *32*, 558-568.
27. Grenoble, D. E.; Voss, R. Materials and designs for implant dentistry. *Biomater Med Devices Artif Organs.* **1976**, *4*, 133-169.
28. Tamimi, F.; Torres, J.; Gbureck, U.; Lopez-Cabarcos, E.; Bassett, D. C.; Alkhraisat, M. H.; Barralet, J. E. Craniofacial vertical bone augmentation: a comparison between 3D printed monolithic monetite blocks and autologous onlay grafts in the rabbit. *Biomaterials.* **2009**, *30*, 6318-6326.
29. Pieri, F.; Lucarelli, E.; Corinaldesi, G.; Aldini, N. N.; Fini, M.; Parrilli, A.; Dozza, B.; Donati, D.; Marchetti, C. Dose-dependent effect of adipose-derived adult stem cells on vertical bone regeneration in rabbit calvarium. *Biomaterials.* **2010**, *31*, 3527-3535.
30. Wang, S.; Zhang, Z.; Zhao, J.; Zhang, X.; Sun, X.; Xia, L.; Chang, Q.; Ye, D.; Jiang, X. Vertical alveolar ridge augmentation with beta-tricalcium phosphate and autologous osteoblasts in canine mandible. *Biomaterials.* **2009**, *30*, 2489-2498.
31. Łączka, M.; Cholewa-Kowalska, K.; Osyczka, A. M. Bioactivity and osteoinductivity of glasses and glassceramics and their material determinants. *Ceram Int.* **2016**, *42*, 14313-14325.
32. Barradas, A. M.; Yuan, H.; van Blitterswijk, C. A.; Habibovic, P. Osteoinductive biomaterials: current knowledge of properties, experimental models and biological mechanisms. *Eur Cell Mater.* **2011**, *21*, 407-429; discussion 429.
33. Yuan, H.; de Bruijn, J. D.; Zhang, X.; van Blitterswijk, C. A.; de Groot, K. Bone induction by porous glass ceramic made from Bioglass (45S5). *J Biomed Mater Res.* **2001**, *58*, 270-276.
34. Miri, A. K.; Muja, N.; Kamranpour, N. O.; Lepry, W. C.; Boccaccini, A. R.; Clarke, S. A.; Nazhat, S. N. Ectopic bone formation in rapidly fabricated acellular injectable dense collagen-Bioglass hybrid scaffolds via gel aspiration-ejection. *Biomaterials.* **2016**, *85*, 128-141.
35. Tang, W.; Lin, D.; Yu, Y.; Niu, H.; Guo, H.; Yuan, Y.; Liu, C. Bioinspired trimodal macro/micro/nano-porous scaffolds loading rhBMP-2 for complete regeneration of critical size bone defect. *Acta Biomater.* **2016**, *32*, 309-323.
36. Meretoja, V. V.; Tirri, T.; Malin, M.; Seppälä, J. V.; Närhi, T. O. Ectopic bone formation in and soft-tissue response to P(CL/DLLA)/bioactive glass composite scaffolds. *Clin Oral Implants Res.* **2014**, *25*, 159-164.
37. Urist, M. R.; Silverman, B. F.; Büring, K.; Dubuc, F. L.; Rosenberg, J. M. The bone induction principle. *Clin Orthop Relat Res.* **1967**, *53*, 243-283.
38. García-Gareta, E.; Coathup, M. J.; Blunn, G. W. Osteoinduction of bone grafting materials for bone repair and regeneration. *Bone.* **2015**, *81*, 112-121.
39. Metzler, P.; von Wilmowsky, C.; Zimmermann, R.; Wiltfang, J.; Schlegel, K. A. The effect of current used bone substitution materials and platelet-rich plasma on periosteal cells by ectopic site implantation: an in-vivo pilot study. *J Craniomaxillofac Surg.* **2012**, *40*, 409-415.
40. Zhao, F.; Lei, B.; Li, X.; Mo, Y.; Wang, R.; Chen, D.; Chen, X. Promoting in vivo early angiogenesis with sub-micrometer strontium-contained bioactive microspheres through modulating macrophage phenotypes. *Biomaterials.* **2018**, *178*, 36-47.
41. Hench, L. L.; Splinter, R. J.; Allen, W. C.; Greenlee, T. K. Bonding mechanisms at the interface of ceramic prosthetic materials. *J Biomed Mater Res.* **1971**, *5*, 117-141.

Received: August 21, 2020
Revised: October 26, 2020
Accepted: October 30, 2020
Available online: December 28, 2020